How to cite: *Angew. Chem. Int. Ed.* **2021**, *60*, 5928–5935
International Edition: doi.org/10.1002/anie.202013489
German Edition: doi.org/10.1002/ange.202013489

Phase Transformation

Stabilization of Undercooled Metals via Passivating Oxide Layers

*Andrew Martin, Boyce S. Chang, Alana M. Pauls, Chuanshen Du, and Martin Thuo**

Abstract: *Undercooling metals relies on frustration of liquid–solid transition mainly by an increase in activation energy. Passivating oxide layers are a way to isolate the core from heterogenous nucleants (physical barrier) while also raising the activation energy (thermodynamic/kinetic barrier) needed for solidification. The latter is due to composition gradients (speciation) that establishes a sharp chemical potential gradient across the thin (0.7–5 nm) oxide shell, slowing homogeneous nucleation. When this speciation is properly tuned, the oxide layer presents a previously unaccounted for interfacial tension in the overall energy landscape of the relaxing material. We demonstrate that 1) the integrity of the passivation oxide is critical in stabilizing undercooled particle, a key tenet in developing heat-free solders, 2) inductive effects play a critical role in undercooling, and 3) the magnitude of the influence of the passivating oxide can be larger than size effects in undercooling.*

Introduction

Advances in miniaturized devices and flexible/wearable electronics, has necessitated a need for low temperature metal processing. Metal processing, however, is largely driven by interconversion between the liquid and solid states at every stage, hence is energetically inefficient.[1] Decoupling the melting from the solidification, through a stabilized metastable state, may eliminate the need for repeated melt-freeze processes.[2] Where this is an undercooled state, solidification can be achieved at a much lower temperature enabling co-processing with/on heat sensitive components or substates. Based on the large volumes (billions of tons)[3] of metals processed per year, a scalable approach to preparing metastable metals is desired.

Metastable materials are ubiquitous dating as far back as utilization of glass in ancient Egypt.[4] Recent advances in solidification kinetics and tuning of alloy composition(s) have led to adoption of Bulk Metallic Glasses (BMG) albeit in niche products.[5] Whereas glassy materials are prevalent, large scale synthesis, stabilization and use of undercooled state[6] is lagging behind. The undercooled state is well studied and understood,[7] but its utility and translation/adoption is only becoming emergent, for example as heat-free solders and composite materials.[8] The main challenge has been lack of an economically-viable scalable method(s) to prepare stable undercooled metal particles. This problem is largely due to the arduous need to eliminate homogeneous and heterogeneous nucleant(s). The former is achieved through size minimization or rapid quenching,[6,9] the latter is achieved via isolation (so-called container-less approaches), albeit only with high-purity isotropic materials.[7e,10] Frustration of homogeneous nucleation can also be achieved by; i) raising the solidification activation barrier (ΔG) beyond stochastic thermal ($k_B T$) fluctuation (Figure 1a), or ii) inhibiting attainment of a critical nuclei radius (r*) (Figure 1a). Given structural similarities between glassy and undercooled states,[11] we infer that with felicitous choice of processing conditions and management of the energy landscape,[12] undercooled metal particles can be stabilized akin to glasses. Herein, we demonstrate the role of thin (nm) passivating oxide(s) and surface chemistry in synthesis and stabilization of undercooled metal particles.

Results and Discussion

In liquid metal droplets, a thin (ca. 0.7–5 nm)[13] passivating oxide layer can introduce unique properties such as non-Newtonian flow (Figure 1b,c).[8,14] The passivating oxide espouses a complex compositional gradient that has, until recently, been ignored.[13a,15] This complex autonomously organized gradient, over a very short distance (a Guggenheim interface),[16] complicates the definition of surface stress and its effect in bulk properties. In the absence of a passivating oxide, the surface energy of a solid metal surface is defined as $\gamma_{metal} = A_H/24\pi D_0^2$, where A_H is Hamaker's constant and D_0 is distance between atoms.[17] A speciated passivating oxide diverges surface tension ($\nabla\gamma$) as the system equilibrates.[13a,15c] Since the oxide shell is a thin,[13] inseparable, yet different, part of the metal particle, the effect of surface tension on the bulk should be considered across its thickness (Figure 1b inset). This inference is based on the understanding that exfoliation of a layer of the oxide triggers reorganization and reactions to restore the equilibrium structure. Ambient removal of an oxide layer is, therefore, not merely a separation as inferred in definition of γ_{metal} above. In liquid metal alloys, therefore, γ_{metal} is at the very least a third rank tensor that captures the contribution of 1) compositional gradient across the thickness of the oxide,[13a,15c,16] 2) shape,[18] 3) component flux/diffusivity,[19] and iv) metal-oxide interface plasticity.[20]

[*] A. Martin, B. S. Chang, A. M. Pauls, C. Du, M. Thuo
Department of Materials Science and Engineering
Iowa State University, Ames, IA 50010 (USA)
E-mail: mthuo@iastate.edu
M. Thuo
Department of Electrical and Computer Engineering
Iowa State University, Ames, IA 50010 (USA)
and
Micro-Electronics Research Centre
Ames, IA 50014 (USA)
Supporting information and the ORCID identification number(s) for the author(s) of this article can be found under: https://doi.org/10.1002/anie.202013489.

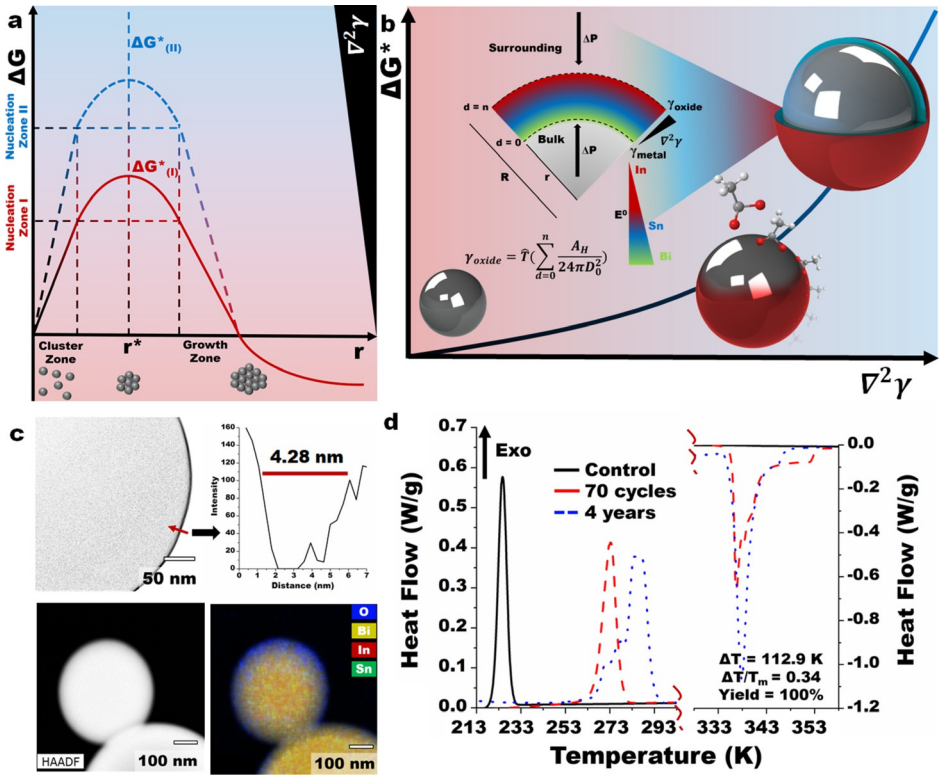

Figure 1. a) Free energy profile as captured by classical nucleation theory and its critical phase transition points. Dotted lines in the y-axis indicate hypothetical regions above which the energy barrier can be overcome stochastically while r* indicates the size of critical nuclei. b) Illustration of the origin and effect of interface tension, and non-PV work, owing to structure of the passivating oxide on the free energy landscape. c) Sobel filter processed HAADF-STEM image of the edge of an undercooled Field's metal particle highlighting oxide thickness (4.3 nm). Whole particle HAADF-STEM and associated EDS map of the particles. d) Truncated DSC trace of freshly made undercooled Field's metal particles and after 70 thermal cycles and after four years of storage on the bench.

Surface speciation, thickness, and packing density across the oxide thickness induces asymmetry in chemical potential across the oxide thickness rendering the interfacial energy a tensor, $\hat{T} \propto \nabla^2\gamma$.[21] Curvature and associated fluctuations in the pressure jump condition (ΔP_{lap}) induce asymmetry in oxidant diffusion on a virgin droplet surface, further extending the rank of the tensor (divergence) needed to describe associated stresses. For brevity and clarity, assume a spherical particle with uniform isotropic compositions across the oxide shell thickness-truncated into hypothetical thin layers. Integrating contributions of in-plane (curvature or compositional undulations) and cross-sectional (primarily due to E^o-driven speciation of elements i to m) differences (Figure 1b) to surface tension across the oxide thickness (d) given the surface area (A) along the distance (z), we can infer a composite interface tension defined as (assuming each layer, n, cleaves uniformly):

$$\gamma_{oxide} = \langle \hat{T} \rangle = \left[\int \int_0^n \left(\sum_i^m \frac{A_H}{24\pi D_0^2} \right)_i dA dz \right] \quad (1)$$

where A_H is Hamaker's constant and D_0 is the distance between two atoms. Since this tension is packed across a very thin (< 5 nm) region (Figure 1c), we infer that these passivating shells embody sharp free energy gradients hence it is a high energy density nanocomponent of the material (Figure 1b).

For a liquid metal to maintain equilibrium, we infer that the bulk must exert work equivalent to the total interfacial tension -free energy equivalent to the Laplace pressure, albeit across a stable, complex, thin oxide.[15a,b] We infer that analogous to the pressure jump condition, this energy tension varies with curvature, hence size. Small liquid metal particles (micron- to nanoscale diameter), therefore, bear a substantial amount of stress due to a combination of Laplace pressure ($\Delta P_{lap} = 2\gamma/r$)[17,20] and the asymmetry (speciation)-driven stress tensor, $\hat{T}$. At equilibrium, we hypothesize that this pressure is accommodated by an approximately equal but opposite amount of interfacial work ($\delta w'$) occurring in the immediate vicinity of the oxide layer.[17] This ansatz is informed by an equilibrium necessitated force balance that is further backed by empirical observation in oxidation-arrested composition inversion.[15a,b] Such a manifestation of tension, therefore, can be tapped to tune energy landscape of a material as it induces asymmetry in chemical potential and component distribution/flux (solid vs. dotted energy curve in Figure 1a).[18]

We hypothesized that by tuning surface architecture of molten metal droplets through the surface oxide, solid–liquid phase transition can be significantly frustrated (in time and/or temperature) by 1) exploiting the self-organizing surface oxide as a container to eliminate heterogeneous nucleation, 2) exploiting the chemical potential gradient to frustrate homogeneous nucleation through a static interfacial stress, $\hat{T}$, and 3) enhance (2) through tunable inductive effect(s) by attaching appropriate ligands on the oxide. This tension must be overcome for Cahn-Hilliard type diffusion to occur,[11b,22] a vital step for critical nuclei formation and eventual crystallization (Figure 1a). We infer that, like entropy and surface stress below r*, this $\hat{T}$, therefore, aids in undercooling-by frustrating solidification (Figure 1b). Considering that the composition and dimensions of the surface oxide can evolve with time,[13b] stimuli, temperature, and oxidant diffusivity,[13a,15] processing conditions and alloy composition (that is, component reactivity) are important in undercooling. Effect of the particle surface on free energy during solidification, ΔG_{LS}, can therefore be captured as $< \nabla \Gamma_i \mu_i >$, where Γ

captures distribution of alloy components in the oxide, analogous to interfacial excess in low vapor pressure components, and μ is chemical potential. It follows that as complexity at the surfaces and interfaces increases, so does the ability to frustrate homogeneous nucleation (high activation energy, ΔG^* Figure 1b), unless the oxide shell growth extends to the Wagner regime where it can trigger nucleation.[23] Analogous theoretical arguments have been made in material response, where metastable interfaces perturb phase transition kinetics as captured in glass transition in BMGs[11b] and in the landscape-inversion phase transition theory (LIPT).[24] We adopt a similar overall energy landscape management approach to synthesize and stabilize undercooled liquid metal droplets. Figure 1d captures stabilization of undercooled Field's metal particles for more than 4 years at ambient conditions (short blue dashes) or repeated thermocycling (long red dashes). Herein, we discuss how we stabilized the particles through surface engineering.

To demonstrate size-dependence, and instability, undercooling in commercially available type 8 SAC305 powder (96.5% Sn, 3% Ag and 0.5% Cu, $T_m \approx 496$ K, 2–8 μm diameter) was analyzed via differential scanning calorimetry (DSC), scanning electron microscopy (SEM) and X-ray diffraction (XRD). In agreement with classical nucleation theory (CNT) and role of surface area-to-volume ratio, solid powder samples ($\approx$3.5 μm average diameter, manufacturer specs 2–11 μm) displays significant degree of undercooling, $\Delta T/T_m = 0.32$, albeit with wide solidification peak (Figure 2a). The native passivating oxide formed on these powders can be assumed to be predominantly SnO_2 with underlying sub-oxide species.[13a,15c] The as-received powder had rough surface (Figure 2b; Supporting Information, Figure S1a), which we infer to be detrimental to undercooling.[8] Thermal aging via repeated cycling (273 K to 523 K at 20 K min^{-1}) of the as-received sample results in rapid loss in both $\Delta T/T_m$ (Figure 2a) and structural integrity of the surfaces (Figure 2b; Supporting Information, Figure S1b). We infer these changes to be a manifestation of repeated expansion-contraction and increased oxidation.[15a,b] Loss in undercooling ($\Delta(\Delta T/T_m) = -0.08$) is not due to any observable size changes as the size

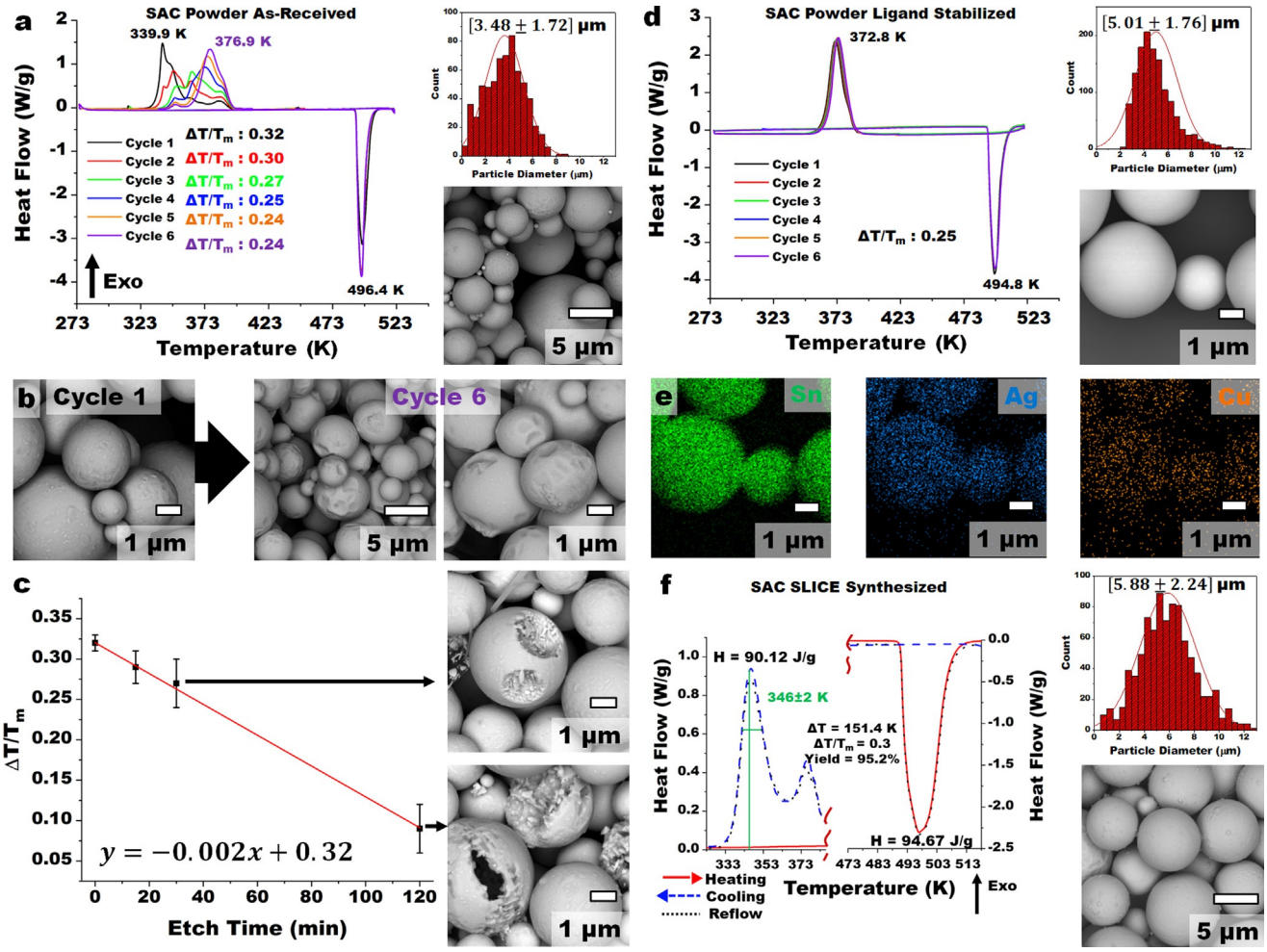

Figure 2. a) DSC heat-cycling of commercial SAC305 powder as received displaying significant loss in undercooling (inset: size distribution and BSE-SEM of the powder). b) SEM of SAC305 powder pre- and post- heating cycle. c) Changes in degree of undercooling owing to surface oxide etching (inset: SEM image of etched powders at different times). d) DSC heat-cycling of ligand stabilized SAC305 powders displaying no change in undercooling (inset: BSE-SEM of the ligand stabilized powder). e) EDS map of the ligand stabilized powder. f) Truncated DSC heat-cycling of SAC305 synthesized using SLICE (inset: size distribution and BSE-SEM of the powder).

distributions is centered around 2–5 μm (Figure 2b), which implies that surface structure might be important in undercooling. We, therefore, infer that observed undercooling in these particles is unstable.

To understand role of the passivating layer in undercooling, the native oxides were thinned, and concomitantly stabilized, by etching with a conjugate acid-base pair (herein CCl_3COO^-/H^+) under ambient condition (Figure 2c). These particles are crystalline at room temperature (Figure S2) and thus surface plasticity that enables reformation of a smooth oxide shell is not possible (that is, irreversible elastic deformation occurs; Supporting Information, Figure S3).[25] Etched samples undergo significant loss in undercooling, with the loss in $\Delta T/T_m$ being proportional to etch time (Figure 2c). Similarly, and as expected, etch time correlates with size of formed surface defects. We infer that; besides a high surface area-to-volume ratio, preservation of a well-defined oxide shell may be critical in maintaining high degree of undercooling.

We desired to stabilize a thin, smooth oxide layer to allow speciation over a short distance and eliminate nucleating edges. For uniformity and continuous re-establishment of asymmetrically etched section of the passivating oxide, plasticity on the metal oxide surface is desired. When the particles are subjected to a conjugate acid–base pair in their molten state (or near T_m) in air, coupled etching–oxidation–chelation reactions occurs leading to a thin (ca. 4 nm) smooth oxide shell.[26] By using dilute (0.1–0.3 M) weak monobasic organic acid in aqueous medium, dissociated carboxylate-hydroxonium ion pairs play complimentary roles. The acid etches (polishes) the oxide layer triggering re-oxidation and regeneration, while the carboxylate chelates both the etched metal ions[27] and the surface of the passivating oxide.[26] Etched metal ions also recruit co-ligands from the media[27] hence, by Le Chatelier's principle, buffers acid dissociation and oxide etch rate. This in situ thinning and polishing of the oxide results in significantly smoother particles (Figure 2d,e and S4). We observe an increase in particle size from 3.5 ± 1.7 μm to 5.0 ± 1.8 μm (Figure 2d) likely due to Ostwald-type ripening during the polishing process. With increase in size, the $\Delta T/T_m$ decreases from 0.32 to 0.25 but is stable to repeated thermal cycling (Figure 2d) compared to the native powder. Thermal cycling does not affect the total liquid content; that is, no loss in undercooling yield (Figure 2a).

For comparison and to avoid the ripening, SAC305 particles were synthesized from bulk using the SLICE (shearing liquid into complex particles) method.[26] This sample was molten and sheared into circa 6 μm particles (Figure 2f) with $\Delta T/T_m = 0.30$ (slightly lower compared to commercial powder due to size). The SLICE method also gave lower yield (95.2%) in the liquid content, comparable to the polished commercial powder (ca. 99%). The synthesized particles have a smooth oxide shell (Figure S5) analogous to the polished commercial powder (Supporting Information, Figure S4) and are also stable under repeated thermal cycling (Supporting Information, Figure S5a). We confirm that the smooth shell is a result of the conjugate acid-base pair by preparing particles in its absence (Supporting Information, Figure S5b). In absence of the acid, particles showed poor undercooling and had a rough surface. We, however, observe that the SLICE-derived sample has a minor product with a freezing peak at 377 K. This product decreases with heat cycling and could be a result of fluctuation in the overall energy landscape basins with thermal stresses.[12a] We infer that a smooth, ligand-stabilized passivating oxide shell leads to stable undercooled state but size likely has a major role in the degree of undercooling. By achieving stable undercooling < 373 K with SAC305, felicitous choice of heat-sensitive substrates for integrated metallic fabrication is unlocked (Supporting Information, Video 1).[14d,28]

To understand the limits of the stabilizing organic shell, we deployed a lower melting ternary alloy, Field's metal (32.5% Bi, 16.5% Sn and 51% In or Bi: 21, In: 60.1, Sn: 18.8 at%, $T_m \approx 335$ K), since it is easier to process and its surface oxide, In_2O_3, has less complicated chemistry compared to tin oxides.[29] Field's metal was also chosen owing to recent interests in its uses[8,14b–d,28,30] and the fact that it can be undercooled well below room temperature for extended periods of time while retaining high liquid content yields (Figure 1d).[8,14c,d] The molten ingot was sheared in aqueous acidic solution (ca. 0.1 M) to give circa 0.9 μm diameter undercooled core–shell particles (Supporting Information, Figure S6) with thin and smooth oxide shell (ca. 4 nm, Figure 1c and S7–8). Particles of various average sizes (from ca. 0.9 ± 0.4 μm to ca. 2.5 ± 0.9 μm) were synthesized to ascertain effect of surface area-to-volume ratio on $\Delta T/T_m$ (Figure 3a). A simple empirical linear relation derived from the fit to the size-dependence of $\Delta T/T_m$ indicates that a particle of about 4.5 μm diameter is needed to retain undercooling below room temperature (Figure 3a). We, however, exercise caution in over interpretation of this simple relation as particle size polydispersity and alloy composition affects the measurements.[28] At about 0.9 μm, we observe that Fields metal is fully undercooled with $> 99\%$ yield and $\Delta T/T_m \approx 0.34$ (Figure 3b).

To evaluate stability of synthesized undercooled particles, accelerated and ambient aging experiments were performed on undercooled Fields metal particles. A sample was subjected to accelerated aging via weekly thermal cycling (200 K to 373 K), 10 cycles per week over the course of 7 weeks (Figure 3c; Supporting Information, Figure S9). During the accelerated aging, this sample showed little to no change in $\Delta T/T_m$ during the first 10 cycles (Figure 3c). This aged sample, however, showed a gradual change in $\Delta T/T_m$ that asymptotes at about 273 K (maximum $\Delta(\Delta T/T_m) = -0.15$). The aging data shows an exponential drop reminiscent of a stochastic decay. We infer that thermal-driven growth in oxide shell,[15a,b] loss of surface ligands, and associated changes in surface morphology (Figure 3c inset and the Supporting Information, Figure S9j) due to repeated expansion and contraction abet the decline in $\Delta T/T_m$. Surface imperfections are a precursor to further oxide growth,[15b] which decreases interface chemical potential gradient per unit volume ($\Delta\mu$ tension) and ultimately $\Delta T/T_m$.[15a] To further support this inference, we observed that when particles were heated to 473 K, total loss of undercooling occurs (Figure 3d). From coupled TGA-IR-MS, loss of surface ligands is observed from 475 K to 573 K (Figure 3d), followed by gradual increase in

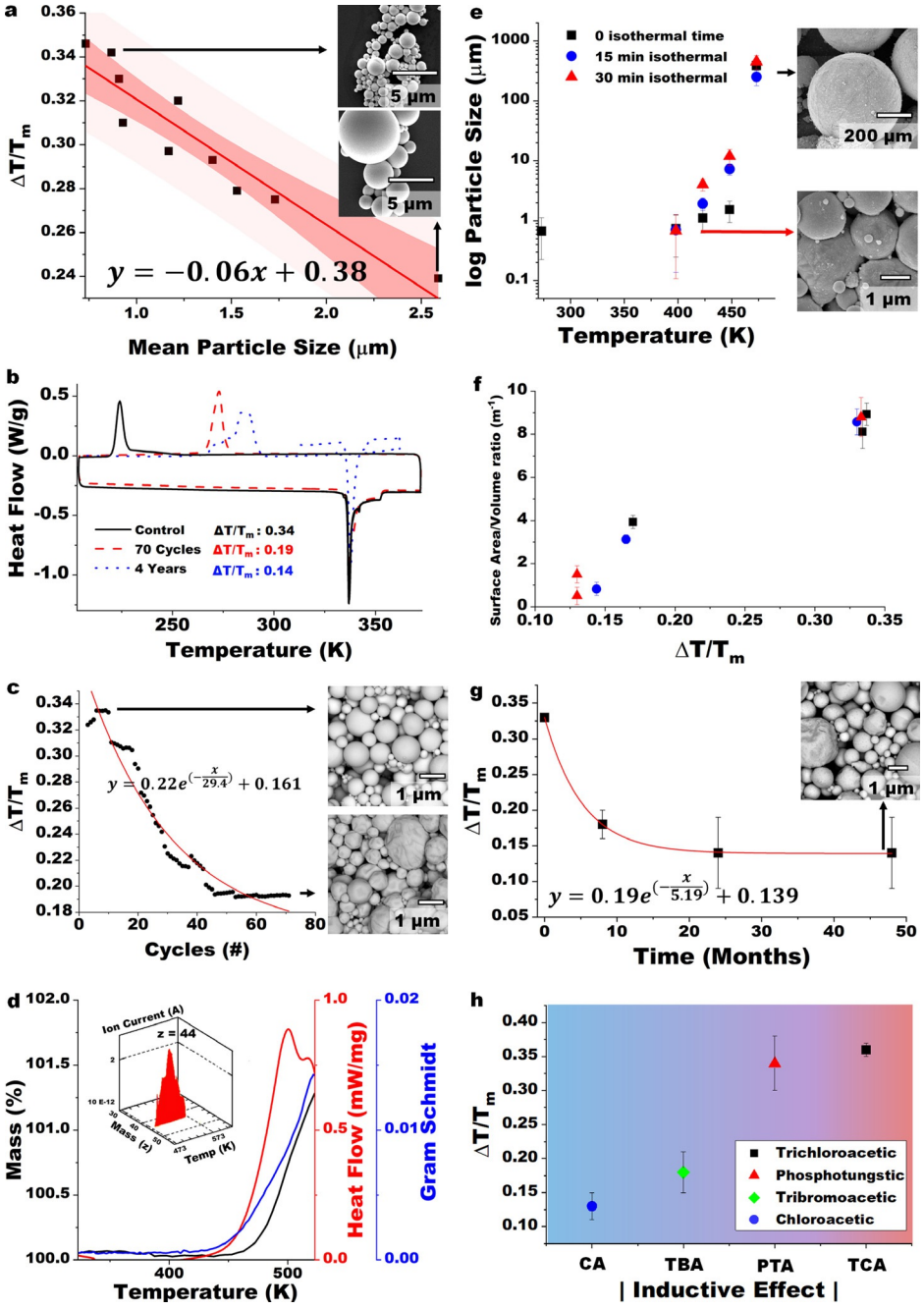

Figure 3. a) Effect of mean particle size towards degree of undercooling. b) DSC trace of undercooled Field's metal particles under different condition illustrating resilience of the undercooling under 3 separate conditions, pristine control particles, particles subjected to 70 heating cycles and particles stored under ambient condition for ca. 4 years. c) Rate of undercooling loss over heating cycles with SEM insets of particles pre- and post- heating cycles. d) TGA-DSC-Gram Schmidt trace for heat treated Field's metal. Inset: MS of heat-treated Field's metal. e) Change in particle size w.r.t temperature and time and f) its effect on surface area to volume ratio and undercooling. g) Rate of undercooling loss in ambient storage over time. h) Changes in degree undercooling with different organic ligands.

mass with heightened oxidation and sintering.[15a,b] Powder X-Ray Diffraction further confirms the loss of undercooling as these particles showed increased crystallinity (Supporting Information, Figure S10). Upon heating to 473 K, an increase in particle size (from the original ca. 0.9 μm) is observed, which is likely due to coalescence with loss of surface ligand and oxide fracture at higher temperatures (Figure 3e; Supporting Information, Figure S11). This rapid increase in size directly affects $\Delta T/T_m$ (Figure 3f).

To analyze stability of this organic layer under ambient condition, a sample (ca. 10 g) was stored in ethyl acetate under ambient conditions (bench top) for >4 years leading to a total loss of $\Delta T/T_m$ from 0.34 to 0.14 (Figure 3g) but without loss in the percentage of particles that remain liquid (Supporting Information, Figure S12). The retention of high liquidous yield in undercooling confirms that the particles are following a similar relaxation pattern irrespective of size hence the decrease in degree of undercooling. Given that the ligands likely form a monolayer on the surface and particles are stored in ethyl acetate, continued slow ligand exchange and vaporization of acetic acid can lead to ligand loss (akin to heating to 473 K) hence destabilization of the oxide shell leading to a lower degree of undercooling. Loss of the ligand could also abet further oxidation of the passivating shell leading to further drop in solidification temperature.[31] Increase in thickness of the oxide gradually hinders oxidant diffusion[31,32] leading to an asymptotic decay in the degree of undercooling (Figure 3g). These data imply that undercooled metal particles are stable against adventitious ambient perturbations over a prolonged period. From this study, we infer that the surface of the particles plays a significant role in the undercooling. Maintaining a smooth, ligand stabilized surface is essential for stable undercooling.

To confirm the role of passivating shell, beyond the well-known and observed size dependency, external perturbation of the overall energy of the oxide was deployed. We investigated effect of ligand inductive effect on degree of undercooling. This study would further inform the role of the interface stress tensor $\langle \hat{T} \rangle$ on undercooling since the ligand

and the metal are not in direct contact. We infer that across the thin (ca. 4 nm) shell, inductive effects on the outer surface of the passivating oxide can perturb energy profile of the metal-oxide interface. Based on successful use of acetic acid with Field's metal ($\Delta T/T_m \approx 0.34$), halogenated analogs and one inorganic acid were investigated (Figure 3h). For simplicity (less speciation across the passivating oxide),[13a,15] a binary eutectic BiSn alloy (Bi: 58, Sn: 42 wt%, or Bi: 44, Sn: 56 at%, $T_m = 411$ K) was used to investigate the role of ligand inductive effects. We observe that increasing inductive effect correlates with higher $\Delta T/T_m$. Increase in $\Delta T/T_m$ with the magnitude, rather than direction, of the inductive effect shows a linear trend for all ligands (Figure 3h). Both positive (phosphotungstic) and negative (haloacetates) inductive effects were investigated (Supporting Information, Figure S13).

To further elaborate the effect of organic ligands used for passivation to the impact on undercooling, different carboxylic acids from C1 (formic) to C6 (hexanoic) were used. Degree of undercooling increases from C0 to C2 and then drops as the carbon chain gets longer, whilst particle sizes remain relatively constant within the 1 µm window (Figure 4a,b; Supporting Information, Figure S14). From Figure 4b we infer that reduction in size does not immediately result in increase in degree of undercooling; rather, high-sphericity, well-polished and passivated surfaces, albeit at larger sizes would tend to have higher degree of undercooling. As longer chain carboxylic acids are employed in synthesis, the condition of the formed particles deteriorates, creating rough surfaces with jagged edges (Supporting Information, Figure S14). Due to the tendency of undercooled liquids to order and form superclusters, these jagged edges can act as nucleation catalyst and reduce the activation energy barrier.[11a,33] Integrating any type of organic passivating layer tends to increase the degree of undercooling due to the increased inductive effect, even if small (Figure 4c). We infer that, due to the nature of the carboxyl ligands, shorter chains would tend to pack better on the curved surface due to limited degree of freedom and thus form the most ideal and equally distributed passivating layer.[34] Formic acid (lowest pK_a), however might be too acidic, hence high etching rate that is detrimental towards the integrity of the native oxide and the metal itself, resulting in significant dealloying (Supporting Information, Figure S14b). Longer chains would also lead to phase transformation into a more independent system (self-assembled monolayer),[34] thus increasing the interfacial distance and reducing the intensity of the chemical potential gradient and mirror charge within the surface oxide.[34]

Using estimation plots, and unpaired mean differences, we compared the effect of size and the combined surface inductive effects. We observed that a 4× change in size leads to an unpaired mean difference (UMD) in undercooling of 0.16 (Figure 4d). Polishing the surface oxide and attaching an acetate ligand, however, leads to a UMD of 0.21 (Figure 4c). Comparing the UMD changes, both size and inductive effects lead to an increase in undercooling, but the surface inductive effect has a larger effect than the commonly known size effect. Comparing the impact over scale, the inductive effects contributed by reducing chain lengths increases the undercooling by about 0.34 nm^{-1} while particle size reduction contribution is about 5.5×10^{-5} nm^{-1}. We infer that the interfacial stress plays a critical role in the undercooling process as such its contribution to the overall free energy relaxation during phase transformation should be considered especially in preparation and use of metal particles/powders.

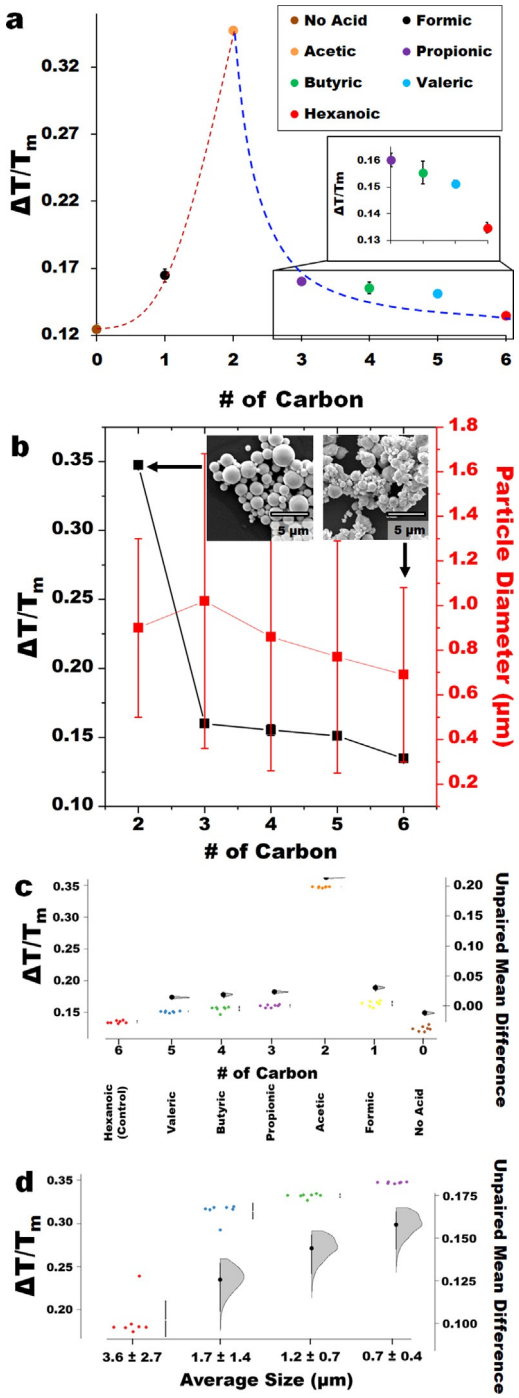

Figure 4. a) Effect of different ligands used to passivate Field's metal particles towards the degree of undercooling (curved lines as eye guides). b) Changes in size vs. undercooling of Field's metal processed using C2–C6 acids. c),d) Estimation plots displaying magnitude of the effect from (c) decrease of inductive effect/increased chain length and (d) increase in particle size towards the degree of undercooling.

Conclusion

This work demonstrates a neoteric approach to frustrating L-S phase transitions by tuning interfacial surface tension of metallic core–shell particles through the surface oxides. We infer that:

1) Undercooled particles can be stabilized via a core–shell architecture in which a thin oxide layer is stabilized with ligands. Surface ligands likely limits chemi- and physisorption on the smooth passivating oxide improving stability. At ambient conditions, majority of the particles remain undercooled for >4 years of storage at ambient conditions.

2) Incorporating all surface work (passivating oxide and nuclei growth) into our general understanding of bulk phase-transition behavior (as captured in classical nucleation theory) opens new pathways to smart material processing of otherwise challenging states.

3) Scalable and accessible synthesis of stable undercooled system enables a distinct class of functional material with unique properties, akin to that of metastable metallic glasses or other amorphous solids. The nature of this frustrated kinetic state creates an opportunity for unprecedented and unique low-energy and low-temperature metal processing pathways (soft lithography, heat-free solders, additive manufacturing, among others).[8,14c,d,16,28,35]

4) From a fundamental science point of view, we extend discourse on classical nucleation theory by highlighting the role of the passivating layer in altering the overall energy state of the bulk. By deductively defining the energy of the passivating oxide as a tensor and a product of component distribution on the surface, we extend the definition of the free energy associated with L-S transformation to:

$$\Delta G_{\mathrm{LS}} = \left[\frac{\Delta H_{\mathrm{f}}\Delta T}{T_{\mathrm{m}}} - \int_{T}^{T_{\mathrm{m}}} \Delta C_{\mathrm{p}}(T)\mathrm{d}T + T\int_{T}^{T_{\mathrm{m}}} \frac{\Delta C_{\mathrm{p}}(T)}{T}\mathrm{d}T\right] - \left[\int_{T}^{T_{\mathrm{m}}} \left(\sum_{i=1}^{n} \Gamma_i \mathrm{d}\mu_i\right)\mathrm{d}T\right] \quad (2)$$

where the last term (added onto the classical equation) captures the role of the outer surface of the particle.

5) By understanding the composition complexity (speciation) across the oxide shell, we expand the definition of the surface energy to capture a Guggenheim interface-a fete that can only be attained by expressing the associated interface energy as, at least, a third rank tensor, $\widehat{\mathrm{T}}$.

Acknowledgements

The authors would like to thank Dr. Lin Zhou (Ames Lab) for the assistance in HAADF-STEM experiments. This work was supported by startup funds from Iowa State University. This work was also supported in part by NSF SBIR grant number 1621910 and Iowa regents innovation fund grant to MT.

Conflict of interest

The authors declare no conflict of interest.

Keywords: energy landscape · inductive effect · metastability · phase transformation · stable undercooling

[1] A. J. Shahani, A. J. Clarke, *MRS Bull.* **2020**, *45*, 906.
[2] D. M. Stefanescu, *Science and Engineering of Casting Solidification*, Springer, Heidelberg, **2015**.
[3] W. S. Association, Global Crude Steel Output Increases by 3.4 % in 2019, https://www.worldsteel.org/media-centre/press-releases/2020/Global-crude-steel-output-increases-by-3.4-in-2019.html. Accessed: August 25, **2020**.
[4] A. Macfarlane, G. Martin, *Glass: a world history*, University of Chicago Press, Chicago, **2002**.
[5] a) H. W. Kui, A. L. Greer, D. Turnbull, *Appl. Phys. Lett.* **1984**, *45*, 615; b) J. Schroers, *Adv. Mater.* **2010**, *22*, 1566; c) M. Telford, *Mater. Today* **2004**, *7*, 36; d) J. Pan, Y. Wang, Q. Guo, D. Zhang, A. Greer, Y. Li, *Nat. Commun.* **2018**, *9*, 1; e) T. A. Waniuk, J. Stevick, S. O'Keeffe, D. J. Stratton, J. C. Poole, M. S. Scott, C. D. Prest (Apple Inc Crucible Intellectual Property LLC), United States Patent US9725796B2, **2012**; f) T. A. Waniuk, J. Stevick, S. O'Keeffe, D. J. Stratton, J. C. Poole, M. S. Scott, C. D. Prest (Apple Inc Crucible Intellectual Property LLC), United States Patent US8813816B2, **2014**.
[6] J. H. Perepezko, J. S. Smith, *J. Non-Cryst. Solids* **1981**, *44*, 65.
[7] a) J. H. Perepezko, *Mater. Sci. Eng.* **1984**, *65*, 125; b) J. H. Perepezko, J. S. Paik, *J. Non-Cryst. Solids* **1984**, *61–62*, 113; c) J. H. Perepezko, J. S. Paik, *MRS Symp. Proc.* **1981**, *8*, 49 (15 pages); d) D. M. Herlach, *Metals* **2014**, *4*, 196; e) D. M. Herlach, *Annu. Rev. Mater. Sci.* **1991**, *21*, 23.
[8] S. Çınar, I. D. Tevis, J. Chen, M. Thuo, *Sci. Rep.* **2016**, *6*, 21864.
[9] a) G. Parravicini, A. Stella, P. Ghigna, G. Spinolo, A. Migliori, F. d'Acapito, R. Kofman, *Appl. Phys. Lett.* **2006**, *89*, 033123; b) P. Shingu, A. Shimohigashi, K. Ishihara in *Rapidly Quenched Metals* (Eds: S. Steeb, H. Warlimont), Elsevier, Amsterdam, **1985**, p. 35 (https://doi.org/10.1016/B978-0-444-86939-5.50015-4).
[10] a) D. M. Herlach, R. F. Cochrane, I. Egry, H. J. Fecht, A. L. Greer, *Int. Mater. Rev.* **1993**, *38*, 273; b) G. Devaud, D. Turnbull, *Mater. Res. Soc. Symp. Proc.* **2011**, *57*, 89; c) G. Devaud, D. Turnbull, *Appl. Phys. Lett.* **1985**, *46*, 844; d) W. Hofmeister, M. Robinson, R. Bayuzick, *Appl. Phys. Lett.* **1986**, *49*, 1342.
[11] a) K. F. Kelton, A. L. Greer in *Solidification of Containerless Undercooled Melts* (Eds: D. Herlach, D. Matson), Wiley-VCH, Weinheim, **2012**, p. 87; b) P. G. Debenedetti, F. H. Stillinger, *Nature* **2001**, *410*, 259.
[12] a) P. G. Debenedetti, F. H. Stillinger, M. S. Shell, *J. Phys. Chem. B* **2003**, *107*, 14434; b) J. C. Mauro, R. J. Loucks, A. K. Varshneya, P. K. Gupta, *Sci. Model Simul.* **2008**, *15*, 241.
[13] a) L. Cademartiri, M. M. Thuo, C. A. Nijhuis, W. F. Reus, S. Tricard, J. R. Barber, R. N. S. Sodhi, P. Brodersen, C. Kim, R. C. Chiechi, G. M. Whitesides, *J. Phys. Chem. C* **2012**, *116*, 10848; b) Z. J. Farrell, C. Tabor, *Langmuir* **2018**, *34*, 234.
[14] a) J. H. Perepezko, J. L. Sebright, P. G. Höckel, G. Wilde, *Mater. Sci. Eng. A* **2002**, *326*, 144; b) M. H. Malakooti, N. Kazem, J. Yan, C. Pan, E. J. Markvicka, K. Matyjaszewski, C. Majidi, *Adv. Funct. Mater.* **2019**, *29*, 1906098; c) B. S. Chang, R. Tutika, J. Cutinho, S. Oyola-Reynoso, J. Chen, M. D. Bartlett, M. M. Thuo, *Mater. Horiz.* **2018**, *5*, 416; d) A. Martin, B. S. Chang, Z. Martin, D. Paramanik, C. Frankiewicz, S. Kundu, I. D. Tevis, M. Thuo, *Adv. Funct. Mater.* **2019**, *29*, 1903687; e) M. D. Dickey, R. C. Chiechi, R. J. Larsen, E. A. Weiss, D. A. Weitz, G. M. Whitesides, *Adv. Funct. Mater.* **2008**, *18*, 1097; f) A. R. Jacob, D. P. Parekh, M. D. Dickey, L. C. Hsiao, *Langmuir* **2019**, *35*, 11774.

[15] a) J. Cutinho, B. S. Chang, S. Oyola-Reynoso, J. Chen, S. S. Akhter, I. D. Tevis, N. J. Bello, A. Martin, M. C. Foster, M. M. Thuo, *ACS Nano* **2018**, *12*, 4744; b) A. Martin, W. Kiarie, B. Chang, M. Thuo, *Angew. Chem. Int. Ed.* **2020**, *59*, 352; *Angew. Chem.* **2020**, *132*, 360; c) R. N. S. Sodhi, P. Brodersen, L. Cademartiri, M. Thuo, C. A. Nijhuis, *Surf. Interface Anal.* **2017**, *49*, 1309.
[16] A. Martin, C. Du, B. Chang, M. Thuo, *Chem. Mater.* **2020**, *32*, 9045 – 9055.
[17] Q. Jiang, Z. Wen, *Thermodynamics of Materials*, Springer, Berlin, **2011**.
[18] J. Lowengrub, J. Xu, A. Voigt, *Fluid Dyn. Mater. Process.* **2007**, *3*, 1.
[19] L.-L. Wang, D. D. Johnson, *J. Am. Chem. Soc.* **2009**, *131*, 14023.
[20] H.-J. Butt, K. Graf, M. Kappl, *Physics and Chemistry of Interfaces*, 3rd ed., Wiley-VCH, Weinheim, **2013**.
[21] J. Lowengrub, J. J. Xu, A. Voigt, *Fluid Dyn. Mater. Process.* **2007**, *3*, 1.
[22] a) L. Anand, *J. Mech. Phys. Solids* **2012**, *60*, 1983; b) C. V. Di Leo, E. Rejovitzky, L. Anand, *J. Mech. Phys. Solids* **2014**, *70*, 1.
[23] a) A. Atkinson, *Mater. Sci. Technol.* **1988**, *4*, 1046; b) Z. Xu, K. M. Rosso, S. Bruemmer, *Phys. Chem. Chem. Phys.* **2012**, *14*, 14534.
[24] a) R. Alert, J. Casademunt, P. Tierno, *Phys. Rev. Lett.* **2014**, *113*, 198301; b) R. Alert, P. Tierno, J. Casademunt, *Nat. Commun.* **2016**, *7*, 13067.
[25] R. Shuttleworth, *Proc. Phys. Soc. London Sect. A* **1950**, *63*, 444.
[26] I. D. Tevis, L. B. Newcomb, M. Thuo, *Langmuir* **2014**, *30*, 14308.
[27] a) B. S. Chang, A. Martin, B. Thomas, A. Li, R. W. Dorn, J. Gong, A. J. Rossini, M. M. Thuo, *ACS Mater. Lett.* **2020**, *2*, 1211; b) B. S. Chang, B. Thomas, J. Chen, I. D. Tevis, P. Karanja, S. Çınar, A. Venkatesh, A. J. Rossini, M. M. Thuo, *Nanoscale* **2019**, *11*, 14060.
[28] A. Martin, C. Du, A. M. Pauls, T. Ward, M. Thuo, *Adv. Mater. Interfaces* **2020**, *7*, 2001294.
[29] M. Batzill, U. Diebold, *Prog. Surf. Sci.* **2005**, *79*, 47.
[30] a) R. K. Kramer, C. Majidi, R. J. Wood, *Adv. Funct. Mater.* **2013**, *23*, 5292; b) T. J. Wallin, J. Pikul, R. F. Shepherd, *Nat. Rev. Mater.* **2018**, *3*, 84; c) M. D. Dickey, *Adv. Mater.* **2017**, *29*, 1606425; d) M. Tavakoli, M. H. Malakooti, H. Paisana, Y. Ohm, D. Green Marques, P. Alhais Lopes, A. P. Piedade, A. T. de Almeida, C. Majidi, *Adv. Mater.* **2018**, *30*, 1801852; e) Z. Zhu, S.-Z. Guo, T. Hirdler, C. Eide, X. Fan, J. Tolar, M. C. McAlpine, *Adv. Mater.* **2018**, *30*, 1707495.
[31] J. T. Law, *J. Phys. Chem.* **1957**, *61*, 1200.
[32] N. Cabrera, N. F. Mott, *Rep. Prog. Phys.* **1949**, *12*, 163.
[33] R. F. Tournier, *Metals* **2014**, *4*, 359.
[34] a) J. Chen, B. Chang, S. Oyola-Reynoso, Z. Wang, M. Thuo, *ACS Omega* **2017**, *2*, 2072; b) J. Chen, Z. Wang, S. Oyola-Reynoso, M. M. Thuo, *Langmuir* **2017**, *33*, 13451.
[35] J. J. Chang, A. Martin, C. Du, A. Pauls, M. M. Thuo, *Angew. Chem. Int. Ed.* **2020**, *59*, 16346 – 16351; *Angew. Chem.* **2020**, *132*, 16488 – 16493.

Manuscript received: October 7, 2020
Revised manuscript received: December 10, 2020
Accepted manuscript online: December 30, 2020
Version of record online: February 4, 2021

